

# DEVELOPMENT OF A MODEL TO INVESTIGATE THE INTERACTION BETWEEN PROCESS AND MACHINE TOOL AND THE RESULTING DYNAMICS OF FRICTION STIR WELDING

F. PANZER\*, M. WERZ\*\* and S. WEIHE\*\*

\* *Institute for Materials Testing, Materials Science and Strength of Materials (IMWF), University of Stuttgart, Germany,  
Orcid Id 0000-0003-1179-6190, Florian.Panzer@imwf.uni-stuttgart.de*

\*\* *Materials Testing Institute (MPA) University of Stuttgart, Germany*

DOI 10.3217/978-3-85125-615-4-31

## ABSTRACT

Friction Stir Welding (FSW) is a solid state joining process where the process and the machine tool used for welding are in direct interaction with each other. This mechanical coupling means that the influence of the machine tool cannot be neglected when investigating FSW: Welds produced on different machines while keeping welding parameters and materials constant are known to show different properties. It is furthermore known that the process forces of FSW have a periodic nature. The reasons for this periodicity, however, are not fully understood yet. It is assumed that properties, like out-of-round-deviations of the spindle, the tool geometry or the stiffness of different machine parts in interaction with the welded material, lead to the characteristics of the FSW forces. Since the welding forces can presumably be employed for online process monitoring, a deeper understanding for the underlying reasons is necessary. In order to investigate this interaction of material and machine as well as the resulting dynamics, a finite element model containing both FSW process and machine, is developed in this work. The process is modeled using the coupled Eulerian-Lagrangian finite-element-formulation. The large strains and strain rates occurring during FSW make it necessary to use an Eulerian formulation for the material to avoid mesh distortion. The ability of the Eulerian formulation to describe the material flow, including free surfaces, furthermore provides the possibility to analyze the formation of volumetric welding defects, which severely reduce the strength of the welds. The tool is modeled using lagrangian elements, a contact is employed to couple the eulerian and lagrangian domains with each other. The machine is modeled in a simplified way using discrete spring elements. The developed model is validated in a first step with welding experiments that were conducted at the IMWF. Second, the model is employed to investigate the interaction between process and machine and therefore the dynamics of FSW. By varying the parameters of the model, the effects, which contribute significantly to the periodic dynamics of FSW, are identified. A simplified 2d-model is employed additionally to analyze the material flow during welding. Another focus lies on the correlation of the process forces and the tool trajectory with defect formation mechanisms. It is shown how flaws in the weld like voids or excessive flash correlate with saliences in the force measurements. These results can not only be employed for monitoring systems but also to improve existing or develop completely new process control strategies.

# Mathematical Modelling of Weld Phenomena 12

Keywords: friction stir welding; process dynamics; process-machine interaction; finite elements; coupled euler-lagrangian method; process forces; online process monitoring

## INTRODUCTION

Friction stir welding (FSW) is a solid state joining process invented 1991 at The Welding Institute (TWI) [1] that is especially suited to join aluminium alloys [2]. A rotating tool consisting of shoulder and pin is plunged into the parts which are to be welded. The friction between tool and material as well as friction in the material itself results in a heating and plasticizing of the parts. After a short dwell time, the tool is moved along the seam line where the combination of rotation and translation of the tool creates the weld. Since no melting of the materials occurs, the resulting weld properties are, especially for aluminium alloys, superior to fusion welding methods. Additionally, it is possible to join dissimilar materials like for example aluminium and steel [3].

The interaction of material and tool during friction stir welding results in process forces as schematically shown in Fig. 1. A force  $F_z$  is necessary to plunge the tool into the materials and maintain the welding position. A torque  $M_z$  is needed to maintain a steady rotational speed. The feed motion during welding results in a force  $F_x$ , additionally, a force  $F_y$  perpendicular to the welding direction occurs.

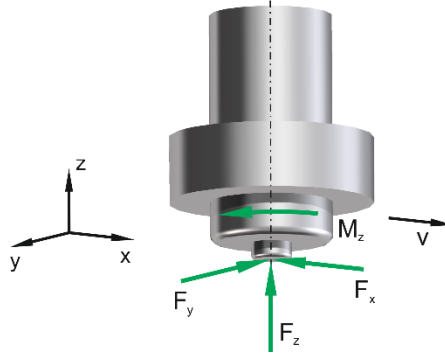


**Fig. 1** Friction stir welding forces

## PROBLEM STATEMENT

The friction stir welding forces have, as shown in Fig. 2, a static part which is superimposed by dynamic effects. Additionally, the friction stir welds show a characteristically banded structure as depicted in Fig. 3. The reasons leading to these periodic force and weld characteristics are not fully understood yet. A variety of theories trying to explain the reasons for the dynamics of friction stir welding exist, however, a systematic investigation still needs to be carried out. The welding force feedback data can presumably be used for the process monitoring of friction stir welding. However, a better understanding of the correlation between the forces and defect formation mechanisms still needs to be gained.

## Mathematical Modelling of Weld Phenomena 12

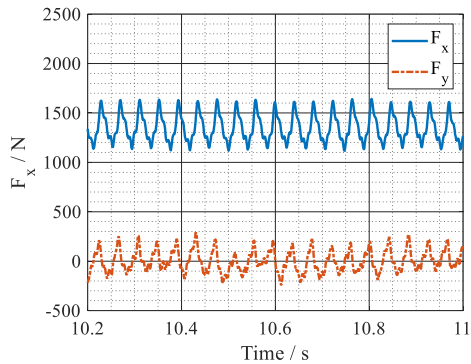


**Fig. 2** Example for friction stir welding forces from experiments

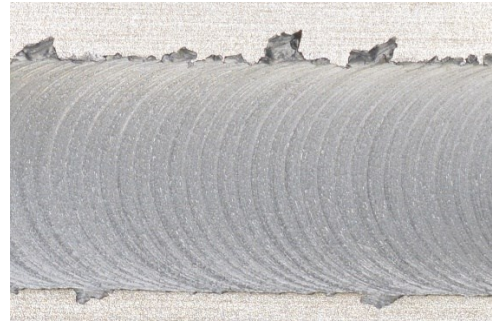


**Fig. 3** Banded structure of a friction stir weld

### OBJECTIVES

The objective of this paper is to gain a better understanding of the dynamics of friction stir welding, i.e., the forces, tool trajectory and resulting weld structure by using a finite element analysis.

To allow a systematic investigation of the friction stir welding dynamics, five hypotheses covering the whole process-machine-system, not only an isolated view of the process, were developed at the IMWF and MPA [4]. Each hypothesis covers a phenomenon that can result in dynamic effects.

In order to investigate which hypotheses, i.e. which effects, contribute significantly to the dynamics of friction stir welding, two finite element models are used.

- A 3d-model is used to complete the main task of the work, i.e. to analyze the welding forces and influence of the machine on the process.
- A geometrically more abstract and simplified 2d-model with a finer mesh is used to analyze the weld formation in vicinity of the pin.

Both models only differ in the geometric setup and mesh size, the simulation methodology is the same for both models.

The 3d-finite element model, as shown in [5], contains the process as well as relevant parts of the machine tool. Starting from a baseline variant, the model is modified to trigger the effects described in the hypotheses intentionally. The comparison of the different model variants shows the reasons for the force characteristics. Additionally, the influence of the machine on the welding results is analyzed. Furthermore, the model is employed to analyze correlations between welding defects and the force responses. This analysis is supported by the results gained from the previous investigations regarding the hypotheses.

The simplified model is used in addition to the process-machine-model in order to observe the material flow in the vicinity of the tool in more detail. A stronger abstraction of the geometry makes it possible to use a finer mesh which is necessary to resolve the material flow patterns.

Compared to experimental procedures, the finite element models offers the advantage that boundary conditions can be prescribed. In this way, features that do not exist in

## Mathematical Modelling of Weld Phenomena 12

experimental environments, like perfectly rigid bearings or tools without any geometrical deviations, can be realized. Furthermore, the weld formation can be observed easily compared to experiments, i.e. a deeper understanding for the underlying mechanisms can be gained.

### LITERATURE REVIEW

This chapter gives a short overview over relevant literature.

#### PROCESS FORCES AND MATERIAL FLOW

As will briefly be shown in this chapter, different theories trying to explain the periodic properties of the friction stir welding forces as well as the banded weld structure exist. A more extensive literature review on the matter can for example be found in [4].

A periodic friction condition between tool and material is postulated in [6] to be the reason for the periodicity of axial force and torque. The authors of [7] list discontinuous movements of dislocations as cause for the periodicity of the torque. In [8] and [9], the dynamic forces of FSW and the banded structure of the welds are explained to result from the interaction of an out-of-round tool movement with the welded material. Analogously, the elliptical motion of the tool in the material resulting from an eccentricity of the tool is stated in [10] to lead to the periodic force properties and banded weld structure of FSW. The elliptical motion of the tool is described to be the result of out-of-round deviations of spindle and tool combined with the flexibility of the machine. The material transport is claimed in [11] to deliver contributions to the periodic parts of the FSW forces in addition to the force parts caused by the interaction of elliptical tool movement and welded material. The tool geometry, more precisely the number of flats on the pin, is found in [12] and [13] to influence the dynamic properties of the FSW forces. Compared to other works, an out-of-round tool movement is not taken into account.

As shown, there are different theories trying to explain the force properties. A thorough investigation, however, still needs to be carried out. What is needed most, is a simulative approach where boundary conditions can be prescribed and, compared to experiments, no unaccounted effects can occur.

A visualization of the material flow during friction stir welding using experimental techniques is difficult. One approach is to use marker materials as presented in [14] and [15]. Another approach is to weld different alloys with each other as shown in [16]. A disadvantage of the experimental techniques using markers or different materials is that the material flow cannot be observed in situ, all analyses have to be done after welding. In [17], welding experiments were done with plasticine instead of metal, in [18], a transparent, visco-plastic material was welded instead of metal. The usage of these alternative materials allows a better observation of the process, however, a comparison of material behavior and especially welding parameters with metals may prove difficult. While no explanations for

## Mathematical Modelling of Weld Phenomena 12

the periodicity of the welds are provided in [14] and [16], the tool eccentricity is listed in [15] and [17] as main reason for the banded structure.

As for the friction stir welding forces, the need for a model to investigate and observe the material flow during friction stir welding is obvious. Again, the possibility to modify and prescribe boundary conditions is important to identify reasons for the friction stir welding dynamics.

### PROCESS MONITORING

The analysis of the frequencies of the FSW forces is used in [13], [19] and [20] for online process monitoring applications. Signs found for welds with flaws are the appearance of frequencies smaller than the rotational frequency of the tool as well as the appearance of multiples thereof. Explanations why certain frequencies are dominant when defects occur are scarcely provided. The two presented models offer a way to analyze the formation of welding defects and find possible explanations for the correlations between force patterns and defects.

### INFLUENCE OF MACHINE ON FRICTION STIR WELDING RESULTS

Mentioned works take the influence of the machine on the welding results only little into account. However, as Fig. 4 shows, the machine has an effect on the welding results. Although identical welding parameters and same aluminium alloys were used, welds manufactured on different machines look distinctly different. In [21] it is assumed that the stiffness of the machine influences the welding results, however, a thorough investigation of the matter was not done. The presented 3d-model offers a way to investigate the influence of machine properties on the welding results without the modification of machine tools or the need to use different machine tools for welding.

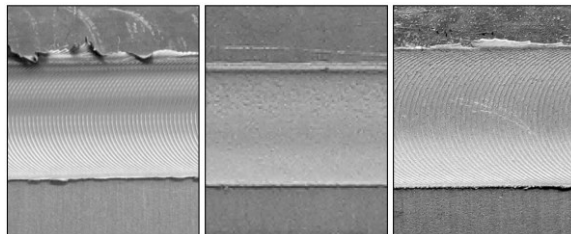


**Fig. 4** Friction stir welds using same FSW parameters and alloys manufactured on different machines [21]

### NUMERICAL SIMULATION OF FRICTION STIR WELDING

The numerical simulation of friction stir welding has been dealt with in a large number of publications. An extensive review can for example be found in [22]. In the following,

references are given for a few works with different modelling approaches towards friction stir welding.

In [23], a computational fluid dynamics (CFD) approach is employed to simulate FSW. A drawback using this approach is that the material behavior can only be modeled as a fluid, but not as a solid. A semi-analytical model that is solved numerically to predict material flow as well as the temperature and slip distribution is presented in [24]. Additionally, a material model suited especially for the simulation of FSW is developed. In [25], FSW is modelled using the Arbitrary Lagrangian-Eulerian (ALE) Finite Element method. This formulation allows a movement of the mesh independent of the material, giving the possibility of adaptive meshing. The large deformations occurring during FSW however reveal the limits of the ALE approach. A relatively new approach to simulate FSW is the Coupled Eulerian-Lagrangian Finite Element method as also used in this work. This approach can cope with the large deformations that occur during FSW and allows the simulation of the welding process including the formation of volumetric defects as well as the calculation of process forces as for example shown in [26] and [27]. A 2d-model using the CEL-method to investigate the material flow during friction stir welding with trigonal pins is developed in [28]. Another possibility to cope with the large deformations is the use of meshfree methods like smoothed particle hydrodynamics (SPH). As shown in [29] or [30], this approach can be used to simulate FSW. An advantage of the SPH formulation is the possibility of parallelization on graphic cards. In [11], a model containing process as well as machine is presented. While the machine is represented numerically with finite elements, the process is modelled using an empirical force model. Using this approach, the impact of welding forces on the machine can be investigated, however, the influence of the machine on welding results cannot be analyzed.

### HYPOTHESES

In order to guarantee a systematic investigation of the dynamics of friction stir welding, the following hypotheses were developed at the IMWF and MPA based on literature review and own experimental results [4] [5]. Each hypothesis covers a phenomenon that can lead to dynamic effects. The whole system consisting of friction stir welding process and machine is considered.

**Hypothesis 1:** Excitation through imbalance. Production tolerances lead to uneven mass distributions. This in return leads to dynamic forces.

**Hypothesis 2:** Excitation through the process. The motion of the tool in the material creates reaction forces. The characteristics of the forces depend on the material properties and the state of the material. When the rotational axis of the spindle and tool does not coincide with the theoretical perfect axis for example, the forced out-of-round motion of the tool in the material causes reaction forces with dynamic properties.

**Hypothesis 3:** Excitation through the tool geometry. Besides tools with circular pins, tools with other pin shapes like e.g. quadratic or triangular are used. The variation of the cross sectional area over time causes forces with dynamic properties. As described before, the forces depend on the material and its state.

**Hypothesis 4:** Excitation through the drive train of the machine. Motor, gearbox and spindle build a mechanical system where vibrations can occur at certain rotational speeds.

## Mathematical Modelling of Weld Phenomena 12

**Hypothesis 5:** In order to produce sound FSW-welds, relatively high axial forces are necessary. The axial forces in combination with the compliance of the machine and the feed motion lead to slip-stick-like effects: The reaction force of the process acts against the feed motion of the machine, i.e. a process-dependent threshold value must be reached in order to enable a feed motion. The compliance of the machine, influenced by the axial force, acts like a spring between process and feed force. Until the spring is loaded, the tool does not move. When the threshold value is reached, a motion is suddenly possible. These slip-stick-like effects cause vibrations when the process-dependent threshold force is suddenly overcome and results in an impulse-like excitation. As mentioned in hypotheses 2 and 3, the forces depend on the material properties and its state.

The focus of investigations in this work lies on the first three hypotheses. Hypothesis 4 and 5 will be investigated in future works.

### MODEL SETUP

As described in the introduction, two different models are used in this work. Both models are set up and solved with Abaqus/Explicit 6.14-3.

The models differ in the geometric setup and mesh size, but not the simulation methodology. The first model is a 3-dimensional model of the process and parts of the machine which is set up according to an available experimental environment. This allows a validation of the model by comparison of calculated and measured forces. A drawback of the model is the need to use a relatively coarse mesh for the welded material in order to achieve reasonable simulation times. The coarse mesh does not allow the analysis of the weld formation in detail. The focus of the model is therefore the analysis of the forces as well as the tool trajectory. Additionally, the 3d-model can be used to investigate the influence of machine properties on the welding process.

In order to be able to investigate the influence of the tool trajectory on the weld formation, a second, simplified 2d-model of the friction stir welding process is used. The usage of strong simplifications allows the use of a finer mesh, however, the calculated forces cannot be compared anymore to the experimental results. The model has therefore more of a supportive character in this work to get qualitative results.

Both models use the same governing equations and description for the material behavior as stated in the next chapter. The differences in the geometry, mesh size and boundary conditions between the two models are described in the following chapters.

### GOVERNING EQUATIONS AND MATERIAL BEHAVIOR

In both model versions, the Coupled Eulerian-Lagrangian (CEL) approach is used to cope with the large deformations that occur during friction stir welding in the material. The mass, momentum and energy conservation equations can be written in the eulerian framework using spatial time derivatives as shown in equations (1) - (3) [27]:

$$\frac{\partial \rho}{\partial t} + \nabla \cdot (\rho v) = 0, \quad (1)$$

$$\frac{\partial \rho \mathbf{v}}{\partial t} + \nabla \cdot (\rho \mathbf{v} \otimes \mathbf{v}) = \nabla \cdot \boldsymbol{\sigma} + \rho \mathbf{b}, \quad (2)$$

$$\frac{\partial e}{\partial t} + \nabla \cdot (e \mathbf{v}) = \boldsymbol{\sigma} : \mathbf{D}, \quad (3)$$

with the material velocity  $\mathbf{v}$ , the density  $\rho$ , the Cauchy stress  $\boldsymbol{\sigma}$ , the vector of body forces  $\mathbf{b}$ , the strain energy  $e$  and the velocity strain  $\mathbf{D}$ . Details on the eulerian formulation, the solution procedure of the governing equations, numerical implementation and contact formulation can be found in [31] and [32].

The usage of eulerian elements for the material avoids mesh distortions which would occur with lagrangian elements. All other parts like the tool, spindle or bearing rings, can be modeled using lagrangian elements. Eulerian linear solid elements with 8 nodes, thermal coupling, reduced integration and hourglass control (EC3D8RT) are used to mesh the material, while the other parts are meshed with lagrangian linear solid elements with also 8 nodes, thermal coupling, reduced integration and hourglass control (C3D8RT). All lagrangian parts are constrained to be rigid bodies in order to save computational costs. Since these parts deform very little compared to the welded sheets, this simplification is justified. In order for thermal contact properties as described below to work, the temperature degree of freedom of the lagrangian parts is not constrained.

The coupling between eulerian and lagrangian domain is realized using a general contact which is available in Abaqus. The Coulomb friction law which relates the frictional shear stress  $\tau$  with the contact pressure  $p$  at the interface as stated in equation (4) is used.

$$\tau = \mu \cdot p \quad (4)$$

A constant friction coefficient of  $\mu = 0.3$  is employed. This value is in accordance with other works [10]. The production of frictional heat through friction between tool and material is taken into account with the ‘‘gap heat generation’’ option of Abaqus. With this option, a fraction of dissipated sliding friction energy can be included as heat source in the analysis. The heat  $q_f$  is calculated using the slip rate  $\dot{\gamma}$  as stated in equation (5) [33]. The default fraction value of  $\eta_f = 1.0$  is used in all analyses.

$$q_f = \eta_f \cdot \tau \cdot \dot{\gamma} \quad (5)$$

The material behavior of the welded aluminum sheets is described using the Johnson-Cook material model [34] which expresses the von Mises flow stress as a function of strain, strain rate and temperature as shown in equation (6):

$$\sigma_y = \left( A + B \cdot \varepsilon_{pl}^n \right) \left( 1 + C \cdot \ln \frac{\dot{\varepsilon}_{pl}}{\dot{\varepsilon}_0} \right) \left( 1 - \frac{T - T_{ref}}{T_m - T_{ref}} \right)^m, \quad (6)$$

## Mathematical Modelling of Weld Phenomena 12

with the equivalent plastic strain  $\varepsilon_{pl}$ , the equivalent plastic strain rate  $\dot{\varepsilon}_{pl}$ , the normalizing strain rate  $\dot{\varepsilon}_0$ , the material solidus temperature  $T_m$  and the reference temperature  $T_{ref}$ .  $A$ ,  $B$ ,  $C$ ,  $n$  and  $m$  are the material model constants.

Due to the dependency on strain, strain rate and temperature, the model is suited for simulations of FSW, for this reason it is also used by other researchers [26] [27]. All simulations in this work were conducted with Johnson-Cook parameters from [10] for EN AW 6061 T6 as listed in Table 1. In Table 2, additionally needed material parameters can be found.

**Table 1** Johnson-Cook parameters for EN AW 6061 T6 [10]

A	B	n	m	C
291 MPa	113 MPa	0.42	1.43	0.006

**Table 2** Additional material parameters

	Density	Young's Modulus	Poisson's Ratio	Thermal Conductivity	Specific Heat
Aluminum	2700 kg/m <sup>3</sup>	70000 MPa	0.33	190 W/(mK)	900 J/(kgK)
Steel	7800 kg/m <sup>3</sup>	210000 MPa	0.3	50 W/(mK)	460 J/(kgK)

In friction stir welding, heat is also produced by internal friction in the material itself, not only by the friction between tool and material [35]. The “inelastic heat-fraction” option of Abaqus allows the inclusion of inelastic energy dissipation as heat source  $q_{pl}$  in the analysis as stated in equation (7) [33]. The default fraction value of  $\eta_{pl} = 0.9$  is used.

$$q_{pl} = \eta_{pl} \cdot \sigma \cdot \dot{\varepsilon}_{pl} \quad (7)$$

### MODEL FOR THE ANALYSIS OF WELDING FORCES AND THE INFLUENCE OF THE MACHINE

The first model, the process-machine-model, consists, as shown in Fig. 5, of the welded sheets, the tool as well as the spindle and the bearings of the machine. The dimensions of the spindle are taken from an ESAB Legio 3ST dedicated FSW machine, which is available at the IMWF respectively MPA for research purposes. The tool used for welding has dimensions as shown in Fig. 6, the welded aluminum sheets have a thickness of 2 mm. In order to capture phenomena like the formation of flash, the thickness of the eulerian mesh is chosen twice the thickness of the sheets. The material is assigned in form of the sheets to the eulerian mesh at the beginning of the simulation.

The stiffness of the bearings is modeled using linear spring elements that connect the bearing rings with the spindle, as schematically shown in Fig. 7. Each bearing is represented

## Mathematical Modelling of Weld Phenomena 12

by four springs to model the behavior in the lateral x- and y-direction. A spring in the axial z-direction in the lower bearing represents the axial stiffness of the bearings.

The welding parameters can be found in Table 3 and are applied as boundary conditions as described in the following. The rotational speed is applied on spindle and tool whereas the boundary conditions for feed speed and heel plunge depth are applied on the bearing rings. The coupling of bearing rings and spindle with the spring elements results in the motion and positioning of the tool. In 0.5 seconds, the tool is plunged into the material realizing the heel plunge depth through the proper plunge feed speed. After a dwell time of 0.5 seconds, the feed speed is applied and two seconds of welding are simulated. In order to realize the tool tilt angle, the whole assembly is rotated. The welded sheets are fixed at the bottom. This is achieved by prescribing a velocity boundary condition of zero in the z-direction. Likewise, the material is prevented from flowing out of the eulerian domain by prescribing a velocity of zero at the edges of the plates in the respective x- and y-directions.

The relatively long simulation time span of 3 seconds for the explicit analysis results in long computation times: About 23 days are needed for one run with 8 cores of an Intel® Xeon® E5-2650 CPU and 128 GB of RAM. In order to speed up the calculations and conduct the presented amount of simulation runs in a reasonable time frame, the density of the material was artificially changed. The time step size of an explicit simulation with solid elements is given by equation (8) [36]:

$$\Delta t = \frac{L_e}{\sqrt{\frac{E \cdot (1 - \nu)}{(1 + \nu) \cdot (1 - 2 \cdot \nu) \cdot \rho}}} \quad (8)$$

with the characteristic length  $L_e$  of the element, the Young's modulus  $E$ , the Poisson's ratio  $\nu$  and the density of the material  $\rho$ . The denominator is the sound speed of the material. The time step size is determined by the size of elements and the density of the materials. A certain mesh size is necessary to discretize the problem in a satisfying level of detail, i.e. the mesh size cannot be chosen at random. For the calculation of welding forces, a mesh size of 0.5 mm is necessary, for the analysis of the weld formation, a finer mesh is needed. The density however can be set deliberately to any value by the user. Through scaling of the density, a larger time step size and therefore a shorter simulation time can be realized. In this work, a scaling factor of  $10^4$  is used which reduces the simulation time from 23 days to about half a day. Since the specific heat is dependent on the mass, cf. Table 2, it must be scaled as well. The scaling is a massive change and it must therefore be ensured that the simulation results can still be used to investigate the presented problem. The impact of the mass scaling is shown in the next chapter.

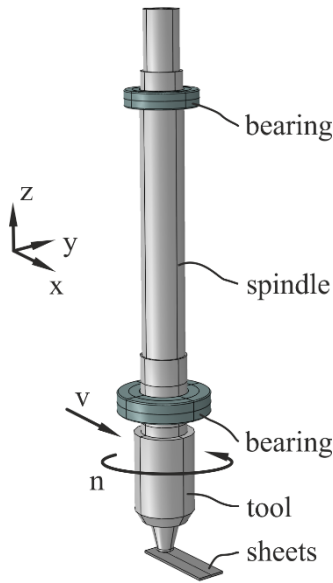


Fig. 5 Process-machine-model

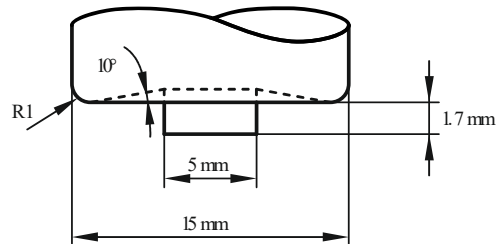


Fig. 6 Tool dimensions

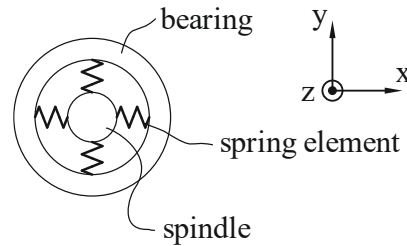


Fig. 7 Schematic of bearing modelling

Table 3 Friction stir welding parameters

Rotational speed	Feed speed	Heel plunge depth	Tilt angle
1500 1/min	1500 mm/min	0.2 mm	1 °

In order to investigate which effects contribute in which amount to the dynamics of friction stir welding, the model is modified. The modifications are done to intentionally trigger the effects described in the hypotheses. The influence of an uneven mass distribution (hypothesis 1) is examined by adding a point mass  $m_p$  at the edge of the tool with a distance  $r$  from the rotational axis as shown in Fig. 8 a. To analyze the impact of an out-of-round tool movement (hypothesis 2), the pin of the tool is moved a distance  $d$  from the rotational axis to an eccentric position as shown in Fig. 8 b. Different pin geometries, namely cylindrical, triangular and quadrangular, as shown in Fig. 8 c, are used to investigate hypothesis 3. As mentioned above are hypothesis 4 and hypothesis 5 not part of the investigations, therefore, no model modifications are needed.

In order to separate effects from welding process and machine, simulations are carried out where no welding is done. This is achieved through a deactivation of the general contact.

All other model properties were kept the same with values as described above. To calculate the frequency responses of the forces, only the welding stage but not the plunging and dwelling phase was taken into account. A sampling rate of 1000 Hz was used for all outputs, additionally an anti-aliasing filter was applied.

## Mathematical Modelling of Weld Phenomena 12

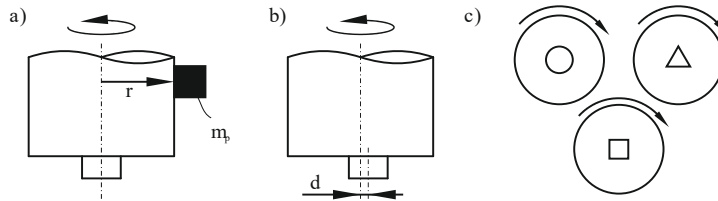


**Fig. 8** Modifications of the process-machine-model to trigger effects of hypotheses

Despite the mass scaling, a mesh size of 0.5 mm is needed with the process-machine-model to reach reasonable computational costs. This mesh size is sufficient to investigate the welding forces, for the investigation of the weld formation in detail however, a finer mesh is necessary. Out of this reason, a simplified 2d-model similar to the one presented in [28] is employed additionally.

### MODEL FOR THE INVESTIGATION OF WELD FORMATION AND MATERIAL FLOW IN DETAIL

The simplified model consists, as shown in Fig. 9, of two welded sheets and a cylinder representing the pin of the tool. The boundary conditions for the rotational speed of the tool as well as feed speed are directly applied on the cylinder representing the pin of the tool.

Only ten revolutions of the tool are simulated. This strong abstraction of the geometry reduces the model size and allows the usage of a much finer element size of 0.1 mm for the eulerian mesh of the material. The CEL-method as implemented in Abaqus does not allow the user to set up two-dimensional models. For this reason, one layer of EC3D8RT elements is used and velocity boundary conditions, as described above, are used to keep the material from flowing out of the eulerian room in all three directions. To this point, no stiffness elements are included. All other properties of the 2d-model are similar to the process-machine-model as described above.

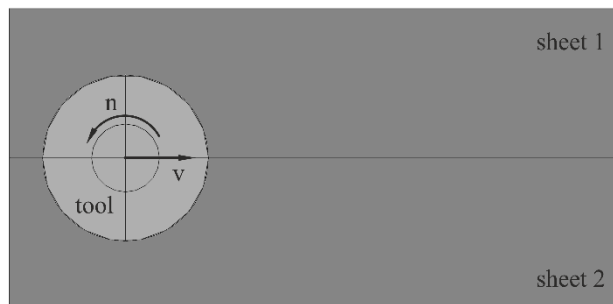


**Fig. 9** 2d-model of friction stir welding

### VALIDATION

In order to investigate the impact of the mass scaling, simulation results are compared to experimental data. Welding experiments where EN AW 6111 T6 sheets were joined using the ESAB Legio 3ST dedicated FSW machine were done at the IMWF and MPA. As shown

in Table 4, the mechanical properties of EN AW 6111 T6 are similar to those of EN AW 6061 T6.

**Table 4** Mechanical properties of EN AW 6061 T6 and EN AW 6111 T6

	Yield strength $R_{p0,2}$	Ultimate tensile strength $R_m$	Total strain at maximum load $A_{gt}$
EN AW 6061 T6 [10]	291 MPa	317 MPa	9.4 %
EN AW 6111 T6 (own tensile tests)	292 MPa	335 MPa	11 %

In the simulations, the heel plunge depth was prescribed in order to achieve a similar plunge depth of the tool between all simulations. The welding experiments were done force-controlled with an axial force  $F_z$  of 6000 N, resulting in an approximately similar heel plunge depth as in the simulations. The other welding parameters, the tool geometry and the sheet thickness were the same as in the model. During welding, the force in welding direction  $F_x$ , the force perpendicular to the welding direction  $F_y$  and the torque around the rotational axis  $M_z$  were measured using a rotating dynamometer called Spike by the company pro-micron.

In addition to the experiments, a simulation without mass scaling was conducted for comparison. All in this chapter presented results were obtained using a model without described modifications and with rigid bearings.

In Fig. 10, the force in welding direction  $F_x$  obtained from the simulation without mass scaling, from the simulation with the aforementioned factor for mass scaling of  $10^4$  as well as from the experiment are shown over a time frame of 0.5 seconds during steady state of welding. Fig. 11 shows the results in the frequency domain.

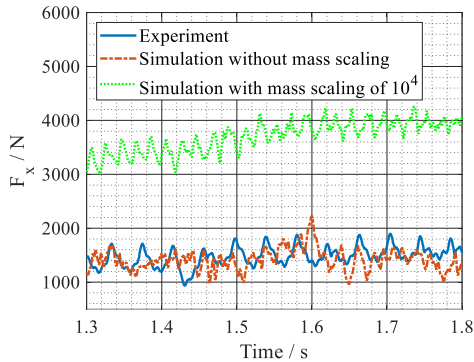


**Fig. 10** Comparison of experiment and simulation in time domain for  $F_x$

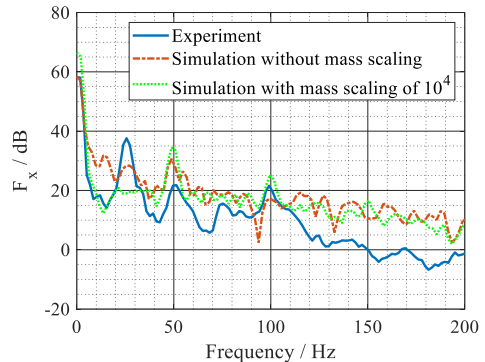


**Fig. 11** Comparison of experiment and simulation in frequency domain for  $F_x$

In the time domain, the results of the simulation without mass scaling are in good accordance with the measurements from the experiment. In the frequency domain it can be seen that the mean values are approximately the same, however, differences can be seen in the dynamic parts. This can be expected since the dynamic forces are part of the investigations conducted in this work. The force calculated with a mass scaling factor of  $10^4$  is higher since the higher density results in a higher mass of the material that is being

extruded during welding. The mean value of the force is about 2.7 times higher when mass scaling is used. This is significantly less than the height of the mass scaling factor of  $10^4$ . An explanation for this circumstance is that only a small amount of material is transported by the tool. This also accounts for the only small differences regarding the height of the amplitudes of the dynamic forces for most frequencies. A larger difference between the two simulations can be seen in the frequency domain at 25 Hz, which is the rotational speed. As will be shown in the next chapters, the peak at this frequency is largely influenced by the modifications of the model, the differences here can be accepted. The results for the torque  $M_z$ , see Fig. 24 and Fig. 25 in the appendix, show similar trends.

Looking at the results it can be concluded that the model can be used to calculate the process forces occurring during friction stir welding. The artificial mass scaling leads to an increase of the process forces, however, general trends are preserved. Through a comparison of the results of different simulations with each other, the reasons for the periodic dynamics of FSW can be identified. It must however be kept in mind that with the employed mass scaling, no absolute, quantitative values can be obtained.

The 2d-model has the purpose to get a deeper understanding of the mechanism of the weld formation in a qualitative way and not to calculate welding forces, therefore, no validation is done for this model. The strong simplifications of the 2d-model would make a validation difficult since welding experiments cannot be set up in the same way.

## RESULTS

In this chapter, the results obtained from the simulations are presented. First, the investigations regarding the first three hypotheses through the modifications of the model are shown. It is furthermore shown how the results change with a change of machine properties, i.e. the spring stiffness of the bearings. Additionally, the 2d-model is employed to analyze the weld formation. Second, correlations between process forces and welding defects are shown using the 3d-model. Mass scaling as described above was used in all presented simulations. The friction stir welding parameters as listed in Table 3 were used if not stated otherwise. Parts of the results can also be found in [5].

### EXCITATION THROUGH IMBALANCE

In Fig. 12, the force in welding direction  $F_x$  is shown in the frequency domain for the unmodified model without imbalance, for a model with an added imbalance mass of 0.1 kg and for a simulation with an added imbalance mass of 1 kg. As first step, the bearings were defined as rigid. Peaks can be seen at multiples of the rotational speed used for welding which is 25 Hz, cf. Table 3. In Table 5 it is listed at which frequencies peaks occur with which amplitudes. In all three model variants, notable peaks occur at 50 Hz, 100 Hz and 150 Hz. Peaks at 25 Hz are only present in the modified models, a significant amplitude occurs only with an imbalance mass of 1 kg. The results for different imbalance masses and flexible bearings with a chosen stiffness of  $5 \cdot 10^6$  N/mm can be seen in Fig. 13. A dominant peak that can be attributed to the bearing stiffness can be seen at 380 Hz. The influence of the bearing stiffness on dynamic force parts with frequencies being multiples of the

## Mathematical Modelling of Weld Phenomena 12

rotational speed is very small, the amplitudes have almost the same height as in the model with rigid bearings, compare also Table 5.

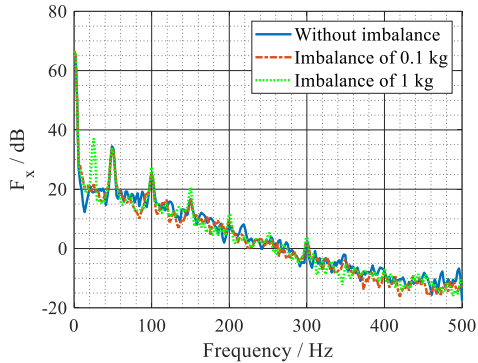


**Fig. 12** Force  $F_x$  in frequency domain for different imbalances with rigid bearings

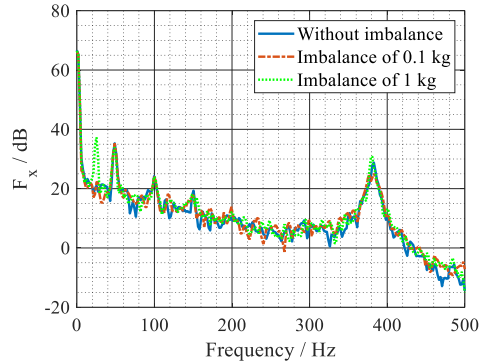


**Fig. 13** Force  $F_x$  in frequency domain for different imbalances with flexible bearings

The force in feed direction  $F_x$  in the frequency domain without welding, i.e. without the influence of the process, for the two different imbalance masses with flexible bearings is shown in Fig. 14. Peaks are present at 25 Hz, 185 Hz and 380 Hz. The peak at the rotational speed is caused by the imbalance mass while the other two peaks can be attributed to the stiffness. A comparison with the simulation with friction stir welding process, Fig. 13 or Table 5, shows that the amplitudes at 25 Hz are approximately the same for the imbalance of 1 kg. This means that the imbalance mass mostly influences the height of the excitation, not the interaction between process and machine. Different amplitudes between welding and no welding at 25 Hz can be seen for the smaller imbalance mass of 0.1 kg. It must however be noted that the peak is barely visible in Fig. 12 respectively Fig. 13, i.e. it may be superimposed by ground level noise.

In Fig. 14, no further dominant peaks can be seen at multiples of the rotational speed, it is therefore concluded that these are caused by the process. The damping introduced into the system through the process may be the reason for the difference of amplitudes at 380 Hz respectively 185 Hz when comparing welding with no welding.

## Mathematical Modelling of Weld Phenomena 12

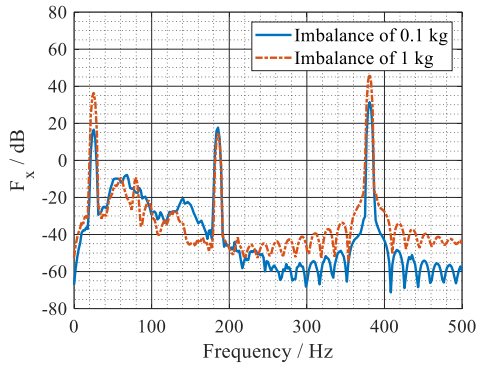


**Fig. 14** Force  $F_x$  in frequency domain for different imbalances without welding with flexible bearings

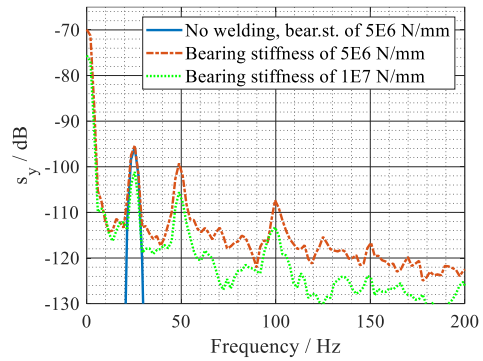


**Fig. 15** Deflection of spindle  $s_y$  without and with welding process with an imbalance of 1 kg

While the simulations show almost no influence of the bearing stiffness, even when comparing rigid with flexible bearings, on the height of the force amplitudes at multiples of the rotational speed, an influence is visible regarding the deflection of the tool. In Fig. 15, the deflection of the spindle without and with welding process for the y-direction with a stiffness of  $5 \cdot 10^6$  N/mm and an imbalance of 1 kg each is shown. In addition, the deflection with welding is shown for an imbalance of 1 kg, but a higher stiffness of  $1 \cdot 10^7$  N/mm. Again, a peak occurs at 25 Hz for all scenarios, while peaks at 50 Hz and 100 Hz can only be seen with friction stir welding process. As for the Force  $F_x$ , the amplitudes at 25 Hz are almost identical for the stiffness of  $5 \cdot 10^6$  N/mm with and without welding. A comparison of the amplitudes between the two different bearing stiffness however shows a difference: The higher stiffness leads to smaller spindle deflections. It can furthermore be seen that the deflection of the spindle during welding has a static part which does not occur without welding. A reason for this could be the differences in the material states between advancing and retreating side of the friction stir weld. The advancing side of the weld is the side where the direction of tool rotation coincides with the welding direction. The retreating side is the side where direction of tool rotation and welding direction are opposite.

### EXCITATION THROUGH THE PROCESS

The results regarding the second hypothesis can be found in Table 5, where the heights of the amplitudes at various frequencies for different simulations are listed. Simulations #8 and #9 as well as #11 and #12 show that for both simulated pin offsets peaks occur at the rotational frequency and multiples thereof. Compared to the first hypothesis, more peaks, for example at 75 Hz and 125 Hz, appear. A higher amplitude compared to the excitation through imbalance can especially be noticed at 25 Hz. Simulations #10 and #13 show the results for the two different pin offsets without welding. A peak occurs at 25 Hz since the pin offset introduces an imbalance into the system. A comparison between the simulations with welding process and without, for example #12 and #13, shows a clear difference in the

## Mathematical Modelling of Weld Phenomena 12

amplitudes at 25 Hz. This means that the interaction between process and eccentric tool has a significant contribution to the dynamics of friction stir welding. Dynamic force parts are caused by the forced eccentric motion of the tool in the material which occur in addition to the dynamic force parts introduced by the pin offset imbalance. The interaction between process and material causes higher amplitudes than the imbalances. As shown above, peaks at harmonics of the rotational frequency occur only with the welding process.

Again, only little differences occur between the models with rigid and flexible bearings (#8 and #9 respectively #11 and #12 in Table 5) when looking at peaks being multiples of the rotational speed. This can also be seen in Fig. 16, where the results for a pin offset of 0.2 mm, but different bearing stiffness of  $1 \cdot 10^6$  N/mm,  $5 \cdot 10^6$  N/mm and  $1 \cdot 10^7$  N/mm are shown. The peaks at 25 Hz, 50 Hz and 75 Hz show almost the same amplitudes. The change of stiffness values has its main impact in a shifting of the right peak to higher frequencies for the higher stiffness value and to lower frequencies for the lower stiffness value.

In all simulations where the FSW process is included, a dominant peak is present independent of the bearing stiffness or other modifications of the model at 50 Hz, i.e. twice the rotational speed. The material transport during FSW is identified in [11] to lead to dynamic forces with twice the frequency of the rotational speed. In Fig. 17, the force  $F_x$  is shown for three simulations with rigid bearings and without modifications, but with three different rotational speeds. Peaks occur at 50 Hz and 100 Hz in all three variants independent of the rotational frequency, which is in contradiction to the aforementioned theory. One explanation could be unaccounted numerical effects, another one the excitation of unaccounted eigenfrequencies of the system. A distinctive peak is present at 80 Hz with a rotational speed of 40 1/s and a small peak is present at 26 Hz in the simulation with 13 1/s as rotational speed. A clear separation of effects, e.g. numerical influences from physical phenomena like material transport must be achieved in future investigations. In order to do so, the 2d-model will be employed. As will be shown in the following, the 2d-model provides a way to visualize and understand the material flow during friction stir welding.

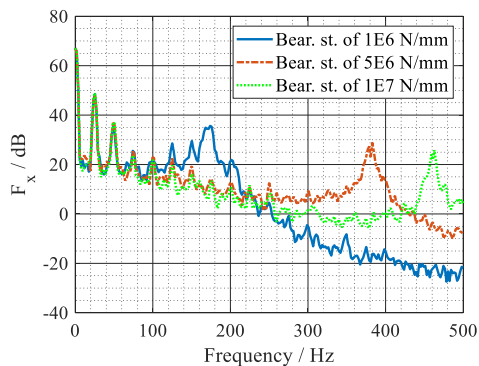


**Fig. 16** Force  $F_x$  in frequency domain for different bearing stiffness with pin offset of 0.2 mm

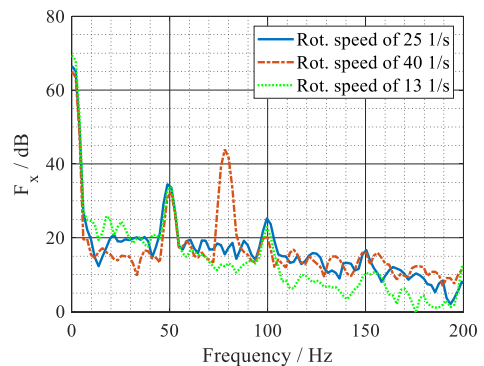


**Fig. 17** Force  $F_x$  in frequency domain for different rotational speeds with rigid bearings

## Mathematical Modelling of Weld Phenomena 12

**Table 5** Comparison of amplitudes of peaks of force  $F_x$  in dB at harmonics of rotational speed for various simulations (bearing stiffness if not rigid:  $5 \cdot 10^6$  N/mm)

#	Hypothesis									
	With process?/Flexible bearings?	25 Hz	50 Hz	75 Hz	100 Hz	125 Hz	150 Hz	300 Hz	350 Hz	425 Hz
1	Yes/No (Baseline model) 1 (0.1 kg)	-	34.5	-	25.2	-	16.7	2.4	-	-
2	Yes/No (Fig. 12) 1 (0.1 kg)	21.7	34.0	-	25.4	-	16.7	2.3	-	-
3	Yes/Yes (Fig. 13) 1 (0.1 kg)	22.3	35.3	-	24.1	-	17.8	-	-	-
4	No/Yes (Fig. 14) 1 (1 kg)	16.6	-	-	-	-	-	-	-	-
5	Yes/No (Fig. 12) 1 (1kg)	37.1	33.8	-	27.4	-	20.6	3.4	-	-
6	Yes/Yes (Fig. 13) 1 (1 kg)	37.3	34.0	-	24.1	-	17.8	-	-	-
7	No/Yes (Fig. 14) 2 (0.03 mm)	36.6	-	-	-	-	-	-	-	-
8	Yes/No	27.6	34.4	22.7	23.1	14.1	19.0	-	-	-
9	2 (0.03 mm) Yes/Yes	27.8	35.5	22.9	24.3	15.7	17.0	9.7	-	-
10	2 (0.03 mm) No/Yes	17.2	-	-	-	-	-	-	-	-
11	2 (0.2 mm) Yes/No	48.7	36.4	24.2	21.8	22.2	15.1	1.9	0.8	-
12	2 (0.2 mm) Yes/Yes	48.1	36.7	25.4	23.0	22.5	19.3	9.4	-	-
13	2 (0.2 mm) No/Yes	27.3	-	-	-	-	-	-	-	-
14	3 (tri.) Yes/Yes	39.0	33.8	32.8	19.6	21.4	26.9	19.5	26.6	18.1
15	3 (quad.) Yes/Yes	18.4	34.6	-	39.3	-	16.7	20.3	29.4	-

In Fig. 18, the results from three simulations with different pin offsets using a mass scaling factor of  $10^6$  are shown. The contour plot shows the eulerian volume fraction (EVF)

of the two different aluminum sheets. The EVF is a value between 0 and 1 and gives the amount of the respective material that is present in an eulerian element, i.e. the material flow of the two sheets caused by the welding process can be visualized. After two or three rotations the process has stabilized and is stationary. While no mixing of the sheets can be seen without pin offset, a banded structure results for both pin offsets. With the larger offset, more material mixing occurs and a slightly different weld geometry results. Without tool offset, material from the lower plate (red) is continuously transported around the tool and deposited behind it. The width of the layer of material that is sheared around the pin does not change. With tool offset, a more batch-wise material transport around the tool takes place. The off-center motion results in a varying width of the material layer moving around the tool. In combination with the varying feed speed, this allows material of the upper plate (blue) to be drawn in behind the tool resulting in the banded structure of the friction stir weld. The distance between the bands is equal to the weld pitch, i.e. the tool advance per revolution of 1 mm. The banded structure is also visible when looking at the plastic strain resulting from the welding process, cf. Fig. 26 in the appendix. No periodic properties however are visible in the temperature distribution as shown in Fig. 27 in the appendix. To the knowledge of the authors no friction stir welds without banded structure exist. It can therefore be assumed that in real-world applications, at least a small off-center motion of the tool must always be present.

The need for the fine mesh of the 2d-model to investigate the material flow is evident from Fig. 28 in the appendix. When using a coarse mesh of 0.5 mm, the weld formation cannot be resolved. A comparison of the force  $F_x$  calculated with the 2d-model with fine and coarse mesh, Fig. 29 in the appendix, shows only little differences. Compared to the 3d-model (Fig. 10), however, the force levels are completely different. A comparison with experimental measured forces is not possible with the 2d-model. One property the two curves (Fig. 16 and Fig. 29) have in common is the dominance of 25 Hz in the dynamic parts of the force when a tool offset is present. This shows that the 2d-model can at least in a qualitative way give information on the dynamic force parts.

More investigations using the 2d-model will be conducted in the future. Especially needed are analyses where the influence of the machine stiffness on the tool trajectory and resulting weld formation is investigated in more detail.

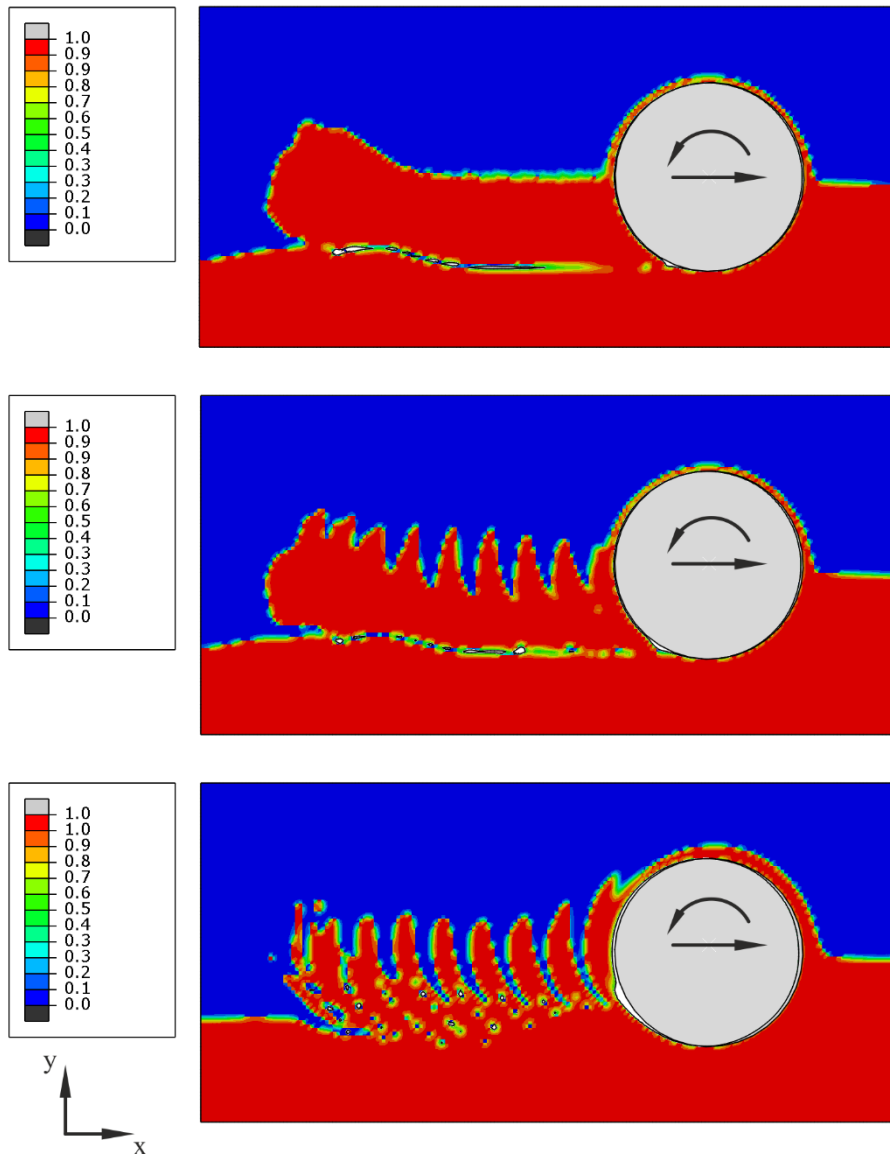


**Fig. 18** Results (eulerian volume fraction) of 2d-model without pin offset (top), with an offset of 0.03 mm (middle) and an offset of 0.2 mm (bottom)

# Mathematical Modelling of Weld Phenomena 12

## EXCITATION THROUGH THE TOOL GEOMETRY

The results for different pin shapes with flexible bearings are also listed in Table 5 under simulations #14 and #15. As for the two hypotheses before, peaks can be found at harmonics of the rotational speed. Compared to the other simulations, notable peaks can also be found at frequencies above 200 Hz. While the triangular pin shows a notable peak at 75 Hz, the quadrangular pin shows a notable peak at 100 Hz. These multiples of the rotational frequency correlate with the number of sides of the respective pin. The strong excitations, especially at higher frequencies, can be attributed to the used pin shapes (Fig. 8 c) which deviate strongly from the circular shape. For other tool shapes, e.g. pins with only small flats on the sides, smaller excitations can be expected.

## CORRELATION OF WELDING DEFECTS AND PROCESS FORCES

In this chapter, two small examples of correlations between FSW defects and welding forces are shown. Additionally, it is demonstrated that the insights from above presented investigations must be considered when developing process monitoring applications based on force feedback data.

### *Tunnel defect*

In Fig. 19, the results from two simulations with two different heel plunge depths are shown. All other welding parameters, material data and boundary conditions were the same. The unmodified baseline model was used, i.e. no dynamic defects were triggered intentionally. The simulation allows a view below the surface of the welded sheets where free surfaces are depicted in grey, allowing a visualization of volumetric defects. Only a small volumetric defect can be seen at beginning of the first weld. The second weld on the contrary shows a tunnel defect on the advancing side along the complete length of the weld caused by the insufficient heel plunge depth of the tool.



**Fig. 19** Simulation of friction stir welds without and with tunnel defect

Fig. 20 shows the frequency domain plot of the force in welding direction  $F_x$  for both welds. Peaks can be seen at 50 Hz and 100 Hz for both welds, however, only the bad weld shows peaks at 25 Hz, 75 Hz and 125 Hz. Taking these results alone, it could be suggested that welds with tunnel defects can be identified using the occurrence of these peaks. However, only when using the model it can be guaranteed that no additional dynamic effects occur. As shown in the chapters before, frequencies being multiples of the rotational speed are caused by imbalance masses, pin offsets or different tool geometries. These effects superimpose the peaks at 25 Hz, 75 Hz and 125 Hz, which indicate the tunnel defect. This in return results in difficulties identifying the bad welds. A solution to that problem

## Mathematical Modelling of Weld Phenomena 12

may lie in the comparison of the height of amplitudes at 25 Hz and 75 Hz, i.e. at the first and third harmonic. Fig. 21 shows the force  $F_x$  for a good and bad weld with tunnel defect, this time with an offset of the tool in both cases. The difference between the two curves is as expected much smaller. The peak at 25 Hz is dominated by the effects of the tool offset resulting in almost identical amplitudes. The impact of the tool offset is less strong at 75 Hz, resulting in different amplitudes. Taking the ratio of the amplitudes at these two frequencies, a criteria for welds with tunnel defects may be defined.

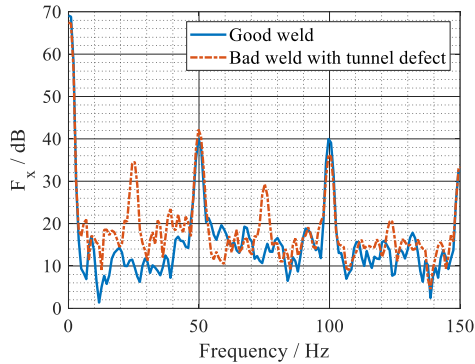


**Fig. 20** Force  $F_x$  in frequency domain for weld without and with tunnel defect, no offset of tool

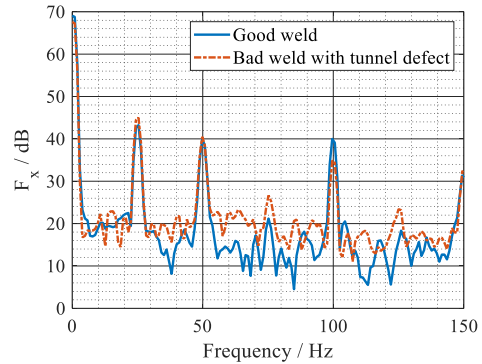
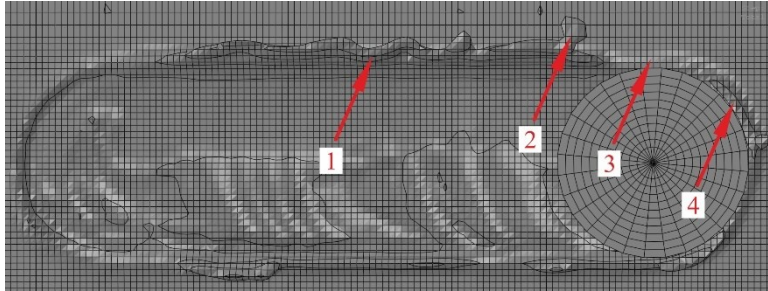


**Fig. 21** Force  $F_x$  in frequency domain for weld without and with tunnel defect, with offset of tool

The same methodology is used in [20] to identify welds with volumetric defects. A ratio of 0.2 between the force amplitudes in welding direction at first and third harmonic of the rotational speed is identified as reliable indicator for volumetric defects with the given experimental setup. The force measurements are additionally used to predict the size of the volumetric defects. The peak at the third harmonic is explained to be caused by the interaction of the three flats of the tool pin with the volumetric defect. Similar trends are found in this work, although a cylindrical pin was used. This shows that further analyses regarding the relation between volumetric defect formation and welding forces are necessary. One way could be the usage of the 2d-model.

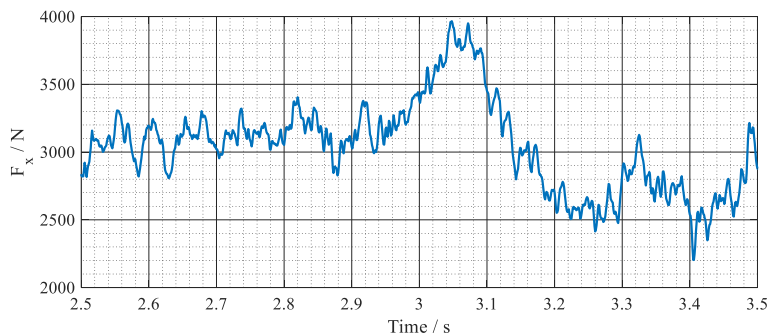
## *Flash formation*

Fig. 22 shows a simulation with strong flash formation caused by a high heel plunge depth. The corresponding force  $F_x$  in the time domain for a time frame of 1 second is shown in Fig. 23.



**Fig. 22** Simulation with flash formation

At the beginning of the weld, flash is continuously formed as indicated (1) in Fig. 22. A relatively steady force level can be seen between 2.5 s and 3 s for this part of the weld in Fig. 23. A larger part of flash is then formed at position (2) and sheared of at position (3). A corresponding peak occurs in the force signal at 3 s, followed by a drop of the force below the initial level at 3.2 s. New flash is formed at position (4) which is accompanied by a rise of the force at the end of the shown time frame. In the frequency domain, no signs could be found indicating the flash formation. The showed correlation could probably be used for monitoring systems. However, it must be known what the force level for a weld without flash looks like. Furthermore, it must be considered that other reasons like the machine stiffness or a change of the heel plunge depth due to thickness variations can also lead to a change of force level. Difficulties will most likely arise in the separation of the different effects.



**Fig. 23** Force  $F_x$  in time domain for weld with flash formation

### SUMMARY AND OUTLOOK

In this work, a finite element model analysis was used to investigate the dynamics of friction stir welding. A systematic variation of the 3d-model was done to verify postulated hypotheses regarding the causes of the FSW dynamics. The 2d-model was used to get additional information on the material flow in the weld.

- Frequencies occurring in the forces are the rotational speed of the tool and its harmonics as well as frequencies which can be attributed to the bearing stiffness. Multiples of the rotational speed can only be seen with welding process, but not without. The frequency of the rotation speed itself, i.e. the first harmonic, is only visible in the modified models.
- The addition of imbalance masses (hypothesis 1) leads to an amplification of the rotational frequency and multiples thereof. The first harmonic is affected most. It is found that the height of amplitudes is almost exclusively influenced by the imbalance mass, but not the interaction of process and tool.
- Tools with pin offset (hypothesis 2) also result in an excitation of the rotational speed and its harmonics. As for the first hypothesis, the pin offset has the strongest impact on the first harmonic. In contrast to the imbalance masses, the interaction of process and out-of-round tool movement is identified as the main reason for the amplification of the frequencies. The forced motion delivers the main contribution to the dynamic force parts while the imbalance introduced through the tool offset only has a minor influence.
- Pin geometries other than cylindrical (hypothesis 3) again result in an excitation of the spindle frequencies and multiples. While a dominant peak is visible at the third harmonic for a triangular pin, a dominant peak can be seen at the fourth harmonic for a quadrangular pin. An excitation is visible over a broader range of frequencies compared to hypothesis 1 and 2.
- Dominant peaks at frequencies which are no multiples of the rotational speed are caused by the stiffness of the bearings. Only a small influence of the stiffness on the force amplitudes being multiples of the rotational frequency can be seen. However, an impact on the tool trajectory is visible: For lower stiffness values, the deflection of spindle and tool gets larger.
- Peaks are visible at 50 Hz and 100 Hz in all simulations, even when the rotational speed is changed. Further analyses are needed to identify if numerical reasons or not yet understood physical phenomena play a role.
- The 2d-model predicts the formation of the characteristic banded structure of friction stir welds for cylindrical pins only for the case when the tool performs an out-of-round movement. A weld without banded structure is only obtained for simulations without tool offset.

The simulations show that correlations between welding defects and welding forces exist and that an identification of defects using force feedback data is principally possible. Tunnel defects may be identified using the ratio of the force amplitudes at first and third harmonic of the spindle frequency. Changes in the force level in the time domain can be employed to identify flash formation. Problems may arise when it comes to a robust implementation of the monitoring systems. Since it must be known how the welding forces look like for a

good weld, it is very likely that a calibration towards the specific environment, i.e. welding machine, tool, parameters and material has to be done for each application.

When comparing the experimental data, Fig. 11, with the forces obtained from the process-machine-model, it can be seen that the results from the simulation with a pin offset of 0.2 mm (Fig. 16) show the best reflection of the overall appearance of the frequency spectrum. The results obtained with the 2d-model regarding the weld structure support that the tool offset plays an important role. The identification of the out-of-round tool movement as main reason for force characteristics and banded weld structure is in accordance with literature [8] [9] [10].

Further work to be done in the future includes simulations without mass scaling to get quantitative results. Simulations superimposing the dynamic effects, especially tool runout and pin geometry, should be carried out. Furthermore, the model needs to be enhanced with additional stiffness elements that represent structural components of the machine. With the enhanced model, the fourth and fifth hypothesis can be investigated. A better understanding of the relation between machine stiffness, tool trajectory and weld formation has to be gained to explain effects as shown in Fig. 4. To do so, the 2d-model can be employed. More investigations to identify numerical influences, for example with varying mesh sizes or different sheet geometries need to be carried out. To get more information for monitoring systems, more simulations with different tool designs and different welding parameters that result in welds with defects have to be done. Another aspect worth looking into is if a possibility exists to couple both finite element model variants.

### ACKNOWLEDGEMENTS

The authors would like to thank the German Research Foundation (Deutsche Forschungsgemeinschaft DFG) for providing funding for the presented research work in scope of the project “Entwicklung eines experimentell gestützten Rührreißschweißmodells zur Festigkeitsvorhersage von Mischverbindungen am Beispiel von Aluminium-Stahl-Verbindungen” (SCHM 746/182-1).

APPENDIX

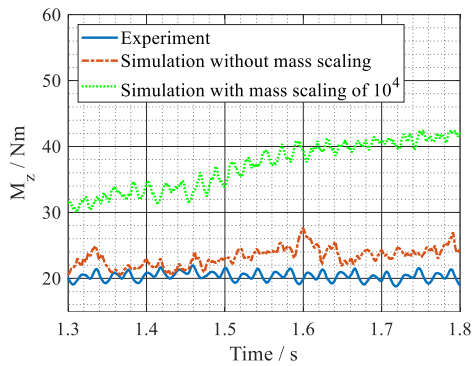


**Fig. 24** Comparison of experiment and simulation in time domain for  $M_z$

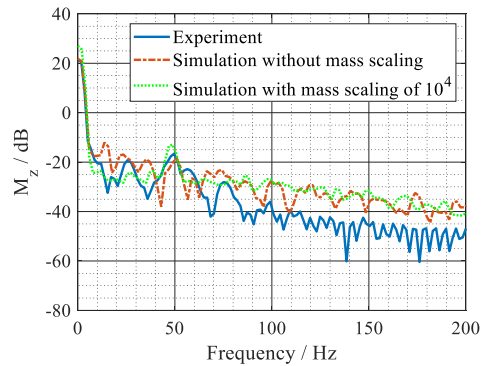


**Fig. 25** Comparison of experiment and simulation in frequency domain for  $M_z$

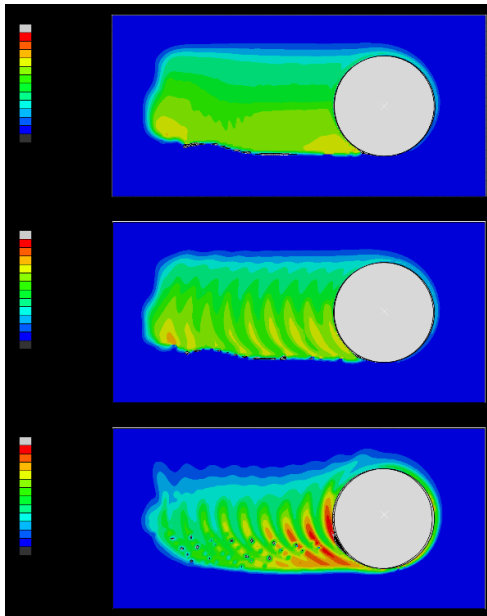


**Fig. 26** Results (volume fraction weighted average equivalent plastic strain) of 2d-model without pin offset (top), with an offset of 0.03 mm (middle) and an offset of 0.2 mm (bottom)

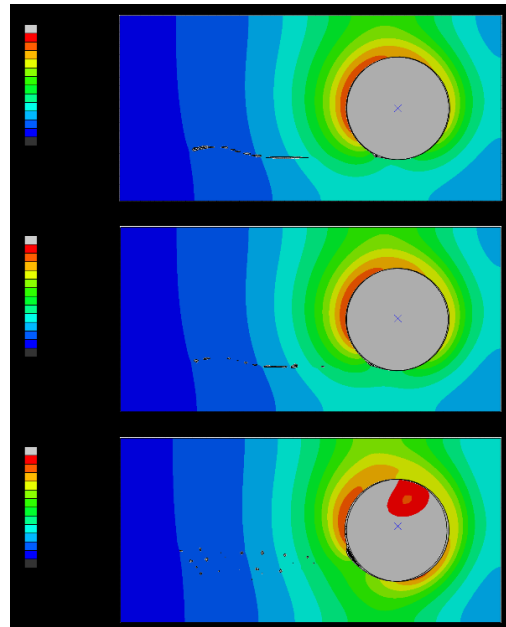


**Fig. 27** Results (temperature) of 2d-model without pin offset (top), with an offset of 0.03 mm (middle) and an offset of 0.2 mm (bottom)

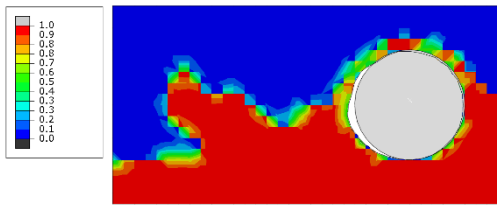


**Fig. 28** Results (eulerian volume fraction) of 2d-model with coarse mesh and pin offset of 0.2 mm

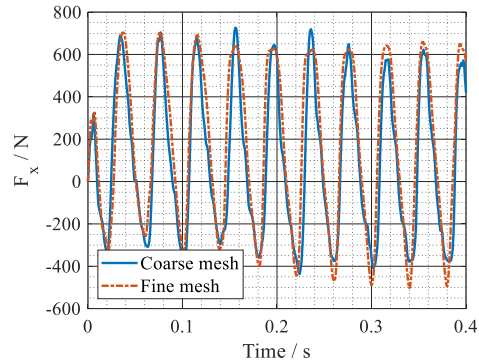


**Fig. 29** Force  $F_x$  in time domain for 2d-model with fine and coarse mesh and a pin offset of 0.2 mm

## REFERENCES

- [1] W. THOMAS, E. NICHOLAS, J. NEEDHAM, M. MURCH, P. TEMPLESMITH, AND C. DAWES, ‘Great Britain Patent G.B. Patent Application No. 9125978.8’, 1991.
- [2] A. K. LAKSHMINARAYANAN, V. BALASUBRAMANIAN, AND K. ELANGO VAN, ‘Effect of welding processes on tensile properties of AA6061 aluminium alloy joints’, *Int. J. Adv. Manuf. Technol.*, vol. 40, no. 3–4, pp. 286–296, 2009.
- [3] M. WERZ AND M. SEIDENFUß, ‘High-Strength Friction Stir Welds for Joining Aluminum and Steel with Dissimilar Sheet Thicknesses’, in *11th International Symposium on Friction Stir Welding, Cambridge*, 2016.
- [4] F. PANZER, M. WERZ, AND S. WEIHE, ‘Experimental investigation of the friction stir welding dynamics of 6000 series aluminum alloys’, *Prod. Eng.*, vol. 12, no. 5, pp. 667–677, 2018.
- [5] F. PANZER, M. WERZ, AND S. WEIHE, ‘Analysis of the oscillating process forces of friction stir welding using finite elements’, in *12th International Symposium on Friction Stir Welding, Chicoutimi*, 2018.
- [6] J. W. QIAN, J. L. LI, J. T. XIONG, F. S. ZHANG, W. Y. LI, AND X. LIN, ‘Periodic variation of torque and its relations to interfacial sticking and slipping during friction stir welding’, *Sci. Technol. Weld. Join.*, vol. 17, no. 4, pp. 338–341, 2012.
- [7] J. T. XIONG *ET AL.*, ‘Characterisation of periodic variation in torque occurred in friction stir welding process’, *Sci. Technol. Weld. Join.*, vol. 19, no. 4, pp. 350–354, 2014.
- [8] J. H. YAN, M. A. SUTTON, AND A. P. REYNOLDS, ‘Processing and banding in AA2524 and AA2024 friction stir welding’, *Sci. Technol. Weld. Join.*, vol. 12, no. 5, pp. 390–401, 2007.
- [9] R. FONDA, A. REYNOLDS, C. R. FENG, K. KNIPLING, AND D. ROWENHORST, ‘Material flow in friction stir welds’, *Metall. Mater. Trans. A Phys. Metall. Mater. Sci.*, vol. 44, no. 1, pp. 337–344, 2013.
- [10] M. HÖBFELD, ‘Experimentelle, analytische und numerische Untersuchungen des Rührreibschweißprozesses’, Universität Stuttgart, 2016.
- [11] M. F. ZAEH AND P. GEBHARD, ‘Dynamical behaviour of machine tools during friction stir welding’, *Prod. Eng.*, vol. 4, no. 6, pp. 615–624, 2010.

- [12] A. SHRIVASTAVA, M. ZINN, N. A. DUFFIE, N. J. FERRIER, C. B. SMITH, AND F. E. PFEFFERKORN, ‘Analysis of Force Transients during Friction Stir Welding’, *43rd Proc. North Am. Manuf. Res.*, vol. XXX, pp. 1–10, 2015.
- [13] A. SHRIVASTAVA *ET AL.*, ‘Physics-based process model approach for detecting discontinuity during friction stir welding’, *Int. J. Adv. Manuf. Technol.*, vol. 79, no. 1–4, pp. 605–614, 2015.
- [14] W. Y. LI, J. F. LI, Z. H. ZHANG, D. L. GAO, AND Y. J. CHAO, ‘Metal Flow during Friction Stir Welding of 7075-T651 Aluminum Alloy’, *Exp. Mech.*, vol. 53, no. 9, pp. 1573–1582, 2013.
- [15] F. C. LIU AND T. W. NELSON, ‘In-situ material flow pattern around probe during friction stir welding of austenitic stainless steel’, *Mater. Des.*, vol. 110, pp. 354–364, 2016.
- [16] X. C. LIU, Y. F. SUN, Y. MORISADA, AND H. FUJII, ‘Dynamics of rotational flow in friction stir welding of aluminium alloys’, *J. Mater. Process. Technol.*, vol. 252, no. October 2017, pp. 643–651, 2018.
- [17] F. GRATECAP, M. GIRARD, S. MARYA, AND G. RACINEUX, ‘Exploring material flow in friction stir welding: Tool eccentricity and formation of banded structures’, *Int. J. Mater. Form.*, vol. 5, no. 2, pp. 99–107, 2012.
- [18] R. KUMAR, V. PANCHOLI, AND R. P. BHARTI, ‘Material flow visualization and determination of strain rate during friction stir welding’, *J. Mater. Process. Technol.*, vol. 255, pp. 470–476, 2018.
- [19] E. BOLDSAIKHAN, E. CORWIN, A. LOGAR, J. MCGOUGH, AND W. ARBEGAST, ‘Detecting Wormholes in Friction Stir Welds from Welding Feedback Data’, in *42nd Midwest Instruction and Computing Symposium*, 2009.
- [20] A. SHRIVASTAVA, M. ZINN, N. A. DUFFIE, N. J. FERRIER, C. B. SMITH, AND F. E. PFEFFERKORN, ‘Force measurement-based discontinuity detection during friction stir welding’, *J. Manuf. Process.*, vol. 26, pp. 113–121, 2017.
- [21] TECHNISCHE UNIVERSITÄT ILMENAU AND UNIVERSITÄT STUTTGART, ‘Untersuchungen zur Übertragbarkeit der Prozessparameter auf Anlagen unterschiedlicher Bauart beim Herstellen von Tailored Blanks auf geschlossener Bahn mittels Rührreibschweißen’, *Forschungsvorhaben AiF-Nr. 14572 N / DVS-Nr. 05.034*, 2007.
- [22] X. HE, F. GU, AND A. BALL, ‘A review of numerical analysis of friction stir welding’, *Prog. Mater. Sci.*, vol. 65, pp. 1–66, 2014.
- [23] Y. ZHU, G. CHEN, Q. CHEN, G. ZHANG, AND Q. SHI, ‘Simulation of material plastic flow driven by non-uniform friction force during friction stir welding and related defect prediction’, *Mater. Des.*, vol. 108, pp. 400–410, 2016.
- [24] M. WERZ AND M. SEIDENFUß, ‘Semi-analytical 1D strain-rate based friction stir welding model for predicting material flow, temperature distribution and slip’, *Math. Model. Weld Phenom.*, vol. 11, 2016.
- [25] H. SCHMIDT AND J. HATTEL, ‘A local model for the thermomechanical conditions in friction stir welding’, *Model. Simul. Mater. Sci. Eng.*, vol. 13, no. 1, pp. 77–93, 2005.
- [26] F. AL-BADOUR, N. MERAH, A. SHUAIB, AND A. BAZOUNE, ‘Coupled Eulerian Lagrangian finite element modeling of friction stir welding processes’, *J. Mater. Process. Technol.*, vol. 213, no. 8, pp. 1433–1439, 2013.
- [27] Z. ZHU, M. WANG, H. ZHANG, X. ZHANG, T. YU, AND Z. WU, ‘A Finite Element Model to Simulate Defect Formation during Friction Stir Welding’, *Metals (Basel)*, vol. 7, no. 7, p. 256, 2017.
- [28] A. TONGNE, C. DESRAYAUD, M. JAHAZI, AND E. FEULVARCH, ‘On material flow in Friction Stir Welded Al alloys’, *J. Mater. Process. Technol.*, vol. 239, pp. 284–296, 2017.

## Mathematical Modelling of Weld Phenomena 12

- [29] W. PAN, D. LI, A. M. TARTAKOVSKY, S. AHZI, M. KHRAISHEH, AND M. KHALEEL, ‘A new smoothed particle hydrodynamics non-Newtonian model for friction stir welding: Process modeling and simulation of microstructure evolution in a magnesium alloy’, *Int. J. Plast.*, vol. 48, pp. 189–204, 2013.
- [30] K. FRASER, L. ST-GEORGES, AND L. I. KISS, ‘Meshfree simulation of the entire FSW process on the GPU’, *11th Int. Symp. Frict. stir Weld.*, no. May, p. 15, 2016.
- [31] D. J. BENSON, ‘A mixture theory for contact in multi-material Eulerian formulations’, *Comput. Methods Appl. Mech. Eng.*, vol. 140, pp. 59–86, 1997.
- [32] D. J. BENSON AND S. OKAZAWA, ‘Contact in a multi-material Eulerian finite element formulation’, *Comput. Methods Appl. Mech. Eng.*, vol. 193, no. 39–41 SPEC. ISS., pp. 4277–4298, 2004.
- [33] DASSAULT SYSTÈMES, ‘Abaqus theory manual 6.10’, 2010.
- [34] G. R. JOHNSON AND W. H. COOK, ‘A constitutive model and data for metals subjected to large strains, high strain rates and high temperatures’, *Proc. 7th Int. Symp. Ballist.*, vol. 21, 1983.
- [35] H. SCHMIDT, J. HATTEL, AND J. WERT, ‘An analytical model for the heat generation in friction stir welding’, *Model. Simul. Mater. Sci. Eng.*, vol. 12, no. 1, pp. 143–157, 2003.
- [36] LIVERMORE SOFTWARE TECHNOLOGY CORPORATION, ‘LS-DYNA Theory manual’, 2006.